

## FAST TRACK COMMUNICATION

# Making tracks in metals

D M Duffy<sup>1,2</sup>, N Itoh<sup>3</sup>, A M Rutherford<sup>1</sup> and A M Stoneham<sup>1</sup>

<sup>1</sup> London Centre for Nanotechnology and Department of Physics and Astronomy, University College London, Gower Street, London WC1E 6BT, UK

<sup>2</sup> EURATOM/UKAEA Fusion Association, Culham Science Centre, Oxfordshire OX14 3DB, UK

<sup>3</sup> 40-202 Koikecho, Meito, Nagoya 465-0047, Japan

Received 16 November 2007, in final form 21 January 2008

Published 7 February 2008

Online at [stacks.iop.org/JPhysCM/20/082201](http://stacks.iop.org/JPhysCM/20/082201)

## Abstract

Swift heavy ions lose energy primarily by inelastic electronic scattering and, above an energy threshold, electronic losses result in damage to the lattice. Such high energy radiation is beyond the range of validity of traditional cascade simulations, and predictive damage calculations are challenging. We use a novel methodology, which combines molecular dynamics with a consistent treatment of electronic energy transport and redistribution to the lattice, to model how swift heavy ions form damage tracks. We consider a range of material parameters (electron–phonon coupling strength, thermal conductivity and electronic specific heat) and show how these affect the maximum lattice temperature reached and the extent of residual damage. Our analysis also suggests that fission tracks may form in alloys of archaeological interest.

(Some figures in this article are in colour only in the electronic version)

## 1. Introduction

Evolving, and increasingly sophisticated, applications of radiation damage demand more sophisticated and accurate modelling techniques than are currently available. Challenges come from ion implantation with nanoscale control, fission track formation in a range of materials, and materials behaviour under the extreme demands of fusion reactor first walls. Increased predictive power, especially if quantitative, would benefit areas ranging from planned safe life extensions of fission reactors [1] to control of dopant distributions for quantum information processing [2]. Traditional methods for modelling of radiation damage use cascade simulations where the role of the electrons is confined to the interatomic potentials. This type of simulation is inappropriate when there is a very large electronic stopping power, creating substantial local electronic excitation. Such excitation leads to a range of phenomena, including transient energy storage and energy redistribution [3]. High stopping powers occur when swift heavy ions are implanted at GeV energies and when fission fragments give rise to similar stopping powers.

One widely used and effective tool for modelling radiation damage is the binary collision code SRIM [4], which uses the pioneering ideas of Bohr [5] and Lindhard [6, 7] to calculate

the range of high energy ions in solids; however the model does not account for defect recombination or for the redistribution of the electronic energy to the lattice. It cannot, therefore, be used to predict accurate defect distributions. What is required is a model that can include the effects of electronic losses as accurately as the SRIM code, but can also account for the transport and redistribution of the electronic energy to the lattice and follow atomic trajectories as accurately as molecular dynamics.

For a few picoseconds after the passage of a swift heavy ion, the electrons are highly excited. There should be rapid equilibration of the excited electronic distribution, within a few femtoseconds [8], allowing us to assign a local temperature to the excited electronic system. The electronic temperature will be much higher than the lattice temperature, therefore electronic energy transport and energy exchange between the electrons and the lattice will determine timescales for the return to equilibrium. There may be spatial charge separation, resulting in strong Coulomb interactions, but spatial charge neutrality will be recovered rapidly for highly mobile electrons in metallic materials therefore the ‘Coulomb explosion’ is unlikely to result in damage in metals. For non-metals, quite different mechanisms are important, notably based on ideas of self-trapping and energy localization [9].

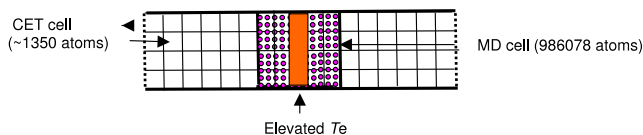


**Figure 1.** Schematic representation of the simulation cell. The swift heavy ion travels vertically through the centre of the cell. The thick black lines represent periodic boundary conditions and the dotted lines represent constant electronic temperature ( $T_e$ ) boundary conditions. The number of coarse-grained electronic temperature (CET) cells has been reduced for clarity.

We recently developed a model which addressed the issue of electronic effects in low energy cascade simulations of radiation damage [10]. Energy lost by the atoms, due to inelastic electronic stopping and electron-ion interactions, is deposited in the electronic system. The electronic energy is transported, via heat diffusion, and redeposited in the lattice by electron-ion interactions. This approach has parallels with those developed recently for modelling sputtering [11] and the melt front motion in overheated metals [12]. We demonstrated that, even for low energy (10 keV) radiation events, the effects of electronic energy redeposition were significant, as the slower cooling resulted in enhanced defect recombination [13]. We also predicted a non-monotonic effect of the electron-phonon coupling strength on the residual damage. Swift heavy ion radiation cannot, however, be simulated directly by atomistic simulations, as the range of such ions is of the order of microns, putting them beyond the range of atomistic simulations for the foreseeable future. Here we extend our earlier methodology to address the problem of very high energy radiation in order to model track formation caused by swift heavy ions.

## 2. Method

We consider the situation where a swift heavy ion has traversed the simulation cell, leaving a trail of highly excited electrons in its wake. Thus the initial condition for the simulation is a column with an elevated electronic temperature, representing the energy lost by an ion with a given stopping power. This electronic energy diffuses through the cell and couples with the lattice, resulting in lattice heating and defect formation. We include the effect of the high electronic temperature by coupling a molecular dynamics (MD) simulation cell to an electronic simulation cell, which was sub-divided into a grid of cubic coarse-grained electronic temperature (CET) cells. The electronic simulation cell was extended in the plane perpendicular to the ion track to permit the transport of electronic energy away from the MD cell. A schematic representation of the coupled simulation cells is shown in figure 1. The model was implemented in the MD code DL-POLY [14] for Fe with a cubic simulation cell (length 22.64 nm, 986078 atoms) interacting via the ‘magnetic potentials’ of Dudarev *et al* [15]. The electronic cell contained  $100 \times 100 \times 9$  CET cells and the central  $9 \times 9 \times 9$  cells were directly coupled to the MD cell.

The simulations aim to model the radiation regime in which the energy loss is deposited primarily in the electronic system (high stopping power regime). The initial electronic temperature can be calculated by assuming that the energy lost by the ion per unit distance (the electronic stopping power) is gained by the electrons in the central column. Thus the initial electronic temperature in the central column of the simulation cell can be estimated from the electronic stopping power of the ion, the cross-section area of the region of elevated  $T_e$  and the electronic specific heat.

In these simulations the initial electronic temperature was taken to be  $7.5 \times 10^4$  K in the central column (cell length 2.52 nm) which corresponds to an electronic stopping power of  $10 \text{ keV nm}^{-1}$ . The electronic temperature ( $T_e$ ) was evolved at each MD timestep via a finite difference solution of the heat diffusion equation on the CET grid. The atomic coordinates were iterated with a leapfrog verlet algorithm, using standard molecular dynamics techniques. Energy was exchanged between the lattice and the electronic system at each MD timestep by means of a Langevin thermostat, with the *local* electron temperature as the thermostat temperature, and a source/sink term in the heat diffusion equation. We demonstrate in [10] that energy lost by the electronic system is gained by the atomic system and vice versa. Three material parameters are required for the heat diffusion equation, the electronic specific heat ( $C_e$ ), the electronic thermal conductivity ( $\kappa$ ) and the electron phonon coupling strength ( $g$ ). We have used a temperature dependence for the electronic specific heat that varies linearly with temperature at low temperatures ( $C_e = \gamma_e T_e$ ), and saturates at the classical value ( $3k_B$ ,  $k_B$  is Boltzmann constant) at around 20000 K. The other material parameters are currently considered to be independent of temperature. We consider a range of coupling strengths ( $\chi = 0.5, 1, 2, \text{ and } 3 \text{ ps}^{-1}$ ), corresponding to electron-ion coupling parameters ( $g = C_1 \chi$  here  $C_1$  is the lattice specific heat) ranging from  $176 \times 10^{16}$  to  $1056 \times 10^{16} \text{ W m}^{-3} \text{ K}^{-1}$ . The electron-ion coupling is related to the mean time between collisions between electrons and phonons. There is considerable uncertainty in this parameter for Fe as there are no experimental measurements. Wang *et al* [16] have used the thermal conductivity to estimate a value of  $g$  of  $130 \times 10^{16} n_e^2 \text{ W m}^{-3} \text{ K}^{-1}$  for Fe, where  $n_e$  is the number of quasi-free electrons per atom. Here we also consider a range of thermal conductivities and specific heat coefficients ( $\gamma_e$ ) in order to investigate the effect of the material parameters on the ion tracks.

## 3. Results and discussion

Figure 2 shows the time evolution of the electronic temperature ( $T_e$ ) and lattice temperature ( $T_l$ ) for the core of the simulation cell for four different coupling strengths. The experimental values for  $\kappa$  and  $\gamma_e$  were used. Three phases can be seen. In phase 1, approximately the first 0.2 ps, there is strong lattice heating. Phase 2 (0.2–0.6 ps) follows the peak in  $T_l$  and in this regime electronic and lattice heat diffusion dominate temperature evolution. In phase 3 there is again significant energy exchange between the electrons and the lattice and

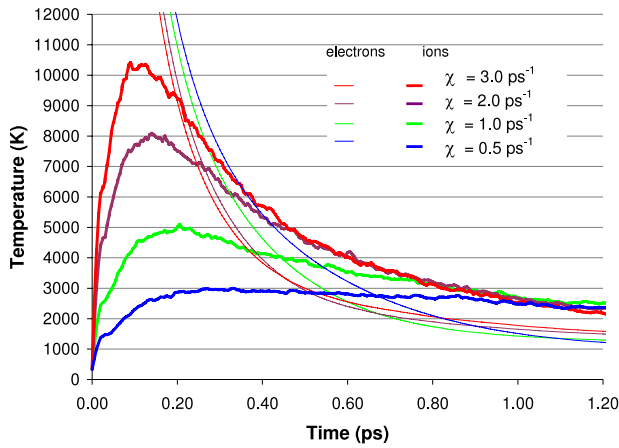


**Figure 2.** Time evolution of  $T_l$  (thick lines) showing lattice heating till about 0.2 ps, heat diffusion for the next 0.4 ps, and electron–lattice energy exchange for the remainder of the simulation. The corresponding evolution for  $T_e$  is shown by thin lines.

**Table 1.** The maximum lattice temperature ( $T_{ml}$ ), the time at which  $T_e = T_l$  ( $t_{equal}$ ), the maximum radius of the melted region ( $R_{melt}$ ), the radius of the residual track ( $R_{defects}$ ) and numbers of stable Frenkel pairs ( $N_{def}$ ).

$\chi$ (ps <sup>-1</sup> )	$T_{ml}$ (K)	$t_{max}$ (ps)	$t_{equal}$ (ps)	$R_{melt}$ (nm)	$R_{defects}$ (nm)	$N_{def}$
0.5	2900	0.39	0.67	0	0	0
1.0	5100	0.21	0.46	1.4	1.4	46
2.0	8100	0.14	0.26	2.0	2.3	66
3.0	10400	0.11	0.20	2.2	2.5	84

$T_e$  decays at a significantly slower rate. The low coupling simulations have lower lattice temperatures in the early stage of the simulation and higher temperatures in the later stages due to slower energy loss to the electronic system.

Table 1 summarizes the results of the simulations for a range of coupling strengths  $\chi$ . In the absence of electronic heat transport, equipartition indicates that the lattice and electronic systems will equilibrate to 37 650 K over a timescale determined by  $\chi$ . The lower maximum lattice temperatures obtained in the simulations indicate that significant diffusion occurs before equilibration is attained. The importance of electronic heat transport is evident also from the estimated diffusion distance  $d(= \sqrt{\alpha_e \tau})$ , with  $\alpha_e$  the high temperature electronic diffusivity  $\kappa_e/C_e = 24 \text{ nm}^2 \text{ ps}^{-1}$ ) of 2.2 nm in 0.2 ps. The lattice heating time ( $t_{max}$ ) and the time at which the electronic temperature falls below the lattice temperature ( $t_{equal}$ ) decrease as  $\chi$  increases. Melting is clearly visible when it occurs, and thermal expansion of the core can also be seen. The maximum radius of the melted region ( $R_{melt}$ ), the radius of the final damaged region ( $R_{defects}$ ) and the numbers of stable Frenkel pairs at the end of the simulation ( $N_{def}$ ) all increase as  $\chi$  increases, as the amount of energy that is redeposited in the lattice increases. As the coupling  $\chi$  varies, the radius of the defect region and the number of defects formed both vary roughly linearly with maximum lattice temperature.

The residual defect configuration for the  $\chi = 1 \text{ ps}^{-1}$  simulation is shown in figure 3. It is clear from this and

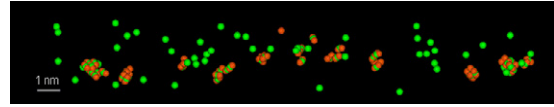


**Figure 3.** The residual defects for the  $\chi = 1 \text{ ps}^{-1}$  simulation. Note the interstitials (gold/dark grey) form clusters and the vacancies (green/light grey) are mostly isolated.

**Table 2.** Results for a range of electronic thermal conductivities  $\kappa$ . Other parameters are defined in table 1.

$\kappa$ (W m <sup>-1</sup> K <sup>-1</sup> )	$T_{ml}$ (K)	$t_{max}$ (ps)	$t_{equal}$ (ps)	$R_{melt}$ (nm)	$R_{defects}$ (nm)	$N_{def}$
20	9140	0.42	0.88	5.8	6.1	122
80	5100	0.21	0.46	1.4	1.4	46
140	3530	0.19	0.34	0.4	1.0	2
200	3000	0.18	0.20	0	0	0

**Table 3.** Results for a range of electronic specific heat coefficient ( $\gamma_e$ ). Other parameters are defined in table 1.

$\gamma_e$ (mJ mol <sup>-1</sup> K <sup>-2</sup> )	$T_{ml}$ (K)	$t_{max}$ (ps)	$t_{equal}$ (ps)	$R_{melt}$ (nm)	$R_{defects}$ (nm)	$N_{def}$
1	5340	0.16	0.27	1.8	1.4	48
5	5100	0.21	0.46	1.4	1.4	46
25	4730	0.19	0.44	1.0	0.9	42

all the other simulations that the residual defects are strongly localized within a radius of a few nanometres of the ion path. The figure also clearly demonstrates a strong tendency for the interstitials to cluster whereas the vacancies are generally isolated. All the other simulations show the same effect. The vacancies are also more spread out in space, contrary to the common situation in which the more mobile interstitials diffuse further than the vacancies. This presumably reflects the unusual highly excited initial state. The presence of the vacancies suggests that these fission tracks might be etched to form nanoscale channels, as is known for non-metal systems.

In order to investigate the effect of thermal transport on the lattice temperature and damage we have carried out further simulations ( $\chi = 1 \text{ ps}^{-1}$ ) for a range of  $\kappa$  (20, 140, 200 W m<sup>-1</sup> K<sup>-1</sup>), in addition to the experimental value of 80 W m<sup>-1</sup> K<sup>-1</sup>. The results are summarized in table 2. We find that varying  $\kappa$  has a significant effect on both  $T_{ml}$  and  $N_{def}$ . Increasing  $\kappa$  to 200 W m<sup>-1</sup> K<sup>-1</sup> from the experimental value resulted in rapid transport in energy away from the core, such that there was insufficient time for a molten zone to develop. Decreased  $\kappa$  resulted in increased disorder and more residual defects. Thus high  $\kappa$  reduces defect formation rather than increases it by quenching, as is sometimes suggested.

Energy storage is higher for materials with high electronic specific heat, so we have examined the effect of higher (25 mJ mol<sup>-1</sup> K<sup>-2</sup>) and lower (1 mJ mol<sup>-1</sup> K<sup>-2</sup>) electronic specific heat coefficient ( $\gamma_e$ ) than the experimental value for Fe (5 mJ mol<sup>-1</sup> K<sup>-2</sup>). In each case we saturate the specific heat at  $3k_B$ , so that only the low temperature values are strongly affected. The results are summarized in table 3. We find that the high  $\gamma_e$  simulation has a lower maximum ionic temperature,

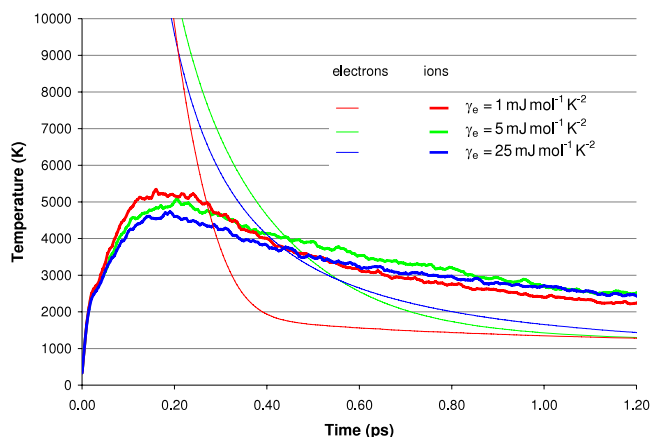


**Figure 4.** Time evolution of  $T_i$  (thick lines) and  $T_e$  (thin lines) for the first 1.2 ps of simulations for 3 values of the electronic specific heat coefficient ( $\gamma_e$ ). Note the rapid decay of  $T_e$  for low  $\gamma_e$ , resulting in faster cooling of the lattice.

resulting in a smaller melted region and fewer residual defects, although the effect is rather small. Perhaps more significantly, at high  $\gamma_e$  we observe a significantly slower decay rate for both  $T_e$  and  $T_i$ , which would lead to enhanced defect annealing. The time dependence of the temperature is shown in figure 4. We note, however, that our treatment of the electronic specific heat is not an accurate representation of energy storage in metals with complex band structures. The approach described for Ni in [17] would give a better description of the temperature dependent parameters.

Swift heavy ion irradiation experiments have been carried out on a range of metals. Some metals (Bi, Ti, Zr, Co and Fe) [18–20] display defect creation above an electronic stopping power (energy loss) threshold whilst others (Ni, Nb, Pt and Pd) [18] experience annihilation of pre-existing defects, but no additional defect production. Some metals display no effect for stopping powers in the experimental range. The results for Fe are particularly interesting as this metal has been shown to exhibit defect annihilation for low stopping power, but defect creation for stopping powers above  $40 \text{ keV nm}^{-1}$  [21]. These experiments have been interpreted in terms of a phenomenological thermal spike model [22], the threshold energy loss for damage creation being presumed just sufficient to raise the *lattice* temperature to the melting temperature. Our simulations show this interpretation is too simple because exceeding the melting temperature does not necessarily lead to melting. However the maximum extent of the molten region does appear to be closely related to the final radius of the track.

In figure 5 we map  $\kappa$  and  $\gamma_e$  for a range of metals. Metals with high  $\kappa$ , and consequently low  $\chi$ , exhibit no effect under swift heavy ion irradiation, whereas metals with low  $\kappa$  exhibit damage creation. Metals with intermediate  $\kappa$  either show defect creation or defect annealing and it appears that annealing is more prevalent in metals with high  $\gamma_e$ . The thermal conductivity results are certainly consistent with our simulations, however we see a smaller effect for  $\gamma_e$  than figure 5 would suggest.

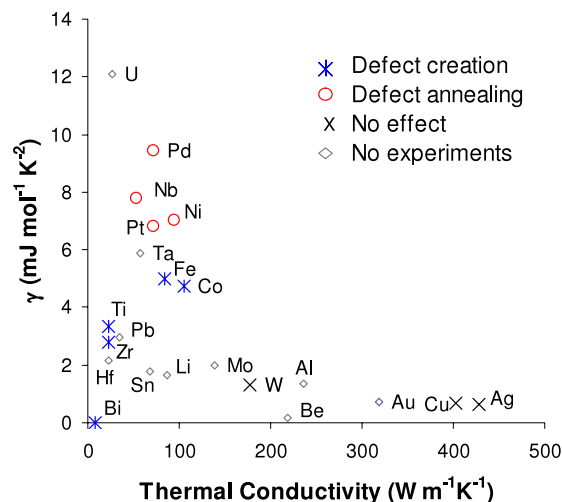


**Figure 5.** Map of the specific heat coefficient ( $\gamma_e$ ) [23] and thermal conductivity ( $\kappa$ ) [24] for common metals. Metals showing defect creation, defect annealing and no effect are represented by stars, circles and crosses, respectively. There are no experimental data for metals shown as diamonds. It appears that  $\kappa$  divides metals in which defects are created or annealed from those in which there is no effect and  $\gamma_e$  divides metals in which defects form from those in which defects are annealed.

Figure 5 enables us to identify metals that should be particularly sensitive to electronic stopping effects. We predict Au, Be and Al to be insensitive whereas Hf, Sn and Pb should be sensitive. U has low  $\kappa$ , and as such should be sensitive and self-irradiation might create tracks, but its high  $\gamma_e$  [25] may favour defect annealing. Since alloying reduces the thermal conductivity, it seems likely that tracks should form in alloys of metals that do not themselves form tracks, including tin and its alloys like pewter and bronze. Thus fission tracks could well form in archaeological artefacts made from such tin alloys and, in principle, at least, might lead to an approach to authentication analogous to geological dating based on fission tracks in apatite.

## 4. Conclusions

Our new approach, by recognizing some of the many roles of electrons in radiation damage, gives a significantly different view of how tracks are created in metals following high local electronic energy losses. Unlike continuum ion-track models, our simulations allow us both to see the extent of core melting and to calculate realistic residual defect configurations. Surprisingly, the ion temperature can exceed the melting temperature without any signs of melting, suggesting that care must be taken when applying thermal spike models. The maximum extent of the melted region does, however, correlate strongly with the final track radius. The electron–ion coupling strength and the thermal conductivity emerge as key parameters for defect creation. It has long been known that excited electrons play an important role in the radiation damage of non-metals [8]. Our example of track formation suggests that excited electrons may have still wider importance.

## Acknowledgments

We acknowledge support of United Kingdom Engineering and Sciences Research Council and the European Communities under the contract of Association between EURATOM and UKAEA. Computer resources on HPCx were provided via our membership of the UK's HPC Materials Chemistry Consortium and funded by EPSRC.

## References

- [1] Stoneham A M, English C A and Phythian W J 1996 *Radiat. Eff. Defects Solids* **144** 311
- [2] Schenkel T, Liddle J A, Persaud A, Tyryshkin A M, Lyon S A, de Sousa R, Whaley K B, Bokor J, Shangkuan J and Chakarov I 2006 *Appl. Phys. Lett.* **88** 112101
- [3] Stoneham A M 1989 *Nucl. Instrum. Methods B* **48** 389
- [4] Ziegler J F, The stopping of ions in solids <http://www.SRIM.org>
- [5] Bohr N 1940 *Phys. Rev.* **58** 654
- [6] Lindhard J, Scharff M and Schiott H E 1963 *Mat. Fys. Medd. Dan. Vidensk. Selsk* **33** 14
- [7] Lindhard J, Nielsen V, Scharff M and Thomsen P V 1963 Notes on Atomic Collisions III *K. Dan. Vidensk. Selk. Mat. Fys. Medd.* **33** (10)
- [8] Bennemann K H 2004 *J. Phys.: Condens. Matter* **16** R995
- [9] Itoh N and Stoneham A M 2001 *Materials Modification by Electronic Excitation* (Cambridge: Cambridge University Press)
- [10] Duffy D M and Rutherford A M 2007 *J. Phys.: Condens. Matter* **19** 016207
- [11] Duvenbeck A and Wucher A 2005 *Phys. Rev. B* **72** 165408
- [12] Ivanov D S and Zhigilei L V 2007 *Phys. Rev. Lett.* **98** 195701
- [13] Rutherford A M and Duffy D M 2007 *J. Phys.: Condens. Matter* **19** 496201
- [14] Smith W and Forester T 1996 *J. Mol. Graph* **14** 135
- [15] Dudarev S L and Derlet P M 2005 *J. Phys.: Condens. Matter* **17** 7097
- [16] Wang X Y, Riffe D M, Lee Y S and Downes M C 1994 *Phys. Rev. B* **50** 8016
- [17] Lin Z and Zhigilei L V 2007 *Appl. Surf. Sci.* **253** 6295
- [18] Dunlop A and Lesueur D 1993 *Radiat. Eff. Defects Solids* **126** 123
- [19] Dunlop A, Legrand P, Lesueur D, Lorenzelli N, Morillo J, Barbu A and Bouffard S 1991 *Europhys. Lett.* **15** 765
- [20] Dufour C, Audouard A, Beuneu F, Dural J, Girard J P, Hairie A, Levalois M, Paumier E and Toulemonde M 1993 *J. Phys.: Condens. Matter C* **5** 4573
- [21] Dunlop A, Lesueur D, Legrand P and Dammak H 1994 *Nucl. Instrum. Methods B* **90** 330
- [22] Wang Z G, Dufour C, Paumier E and Toulemonde M 1994 *J. Phys.: Condens. Matter* **6** 6733
- [23] Kittel C 1996 *Introduction to Solid State Physics* (New York: Wiley)
- [24] Lide D R (ed) 2001 *CRC Handbook of Chemical Physics* 82nd edn (Boca Raton, FL: CRC Press)
- [25] Dempsey C W, Gordon J E and Romer R H 1963 *Phys. Rev. Lett.* **12** 547